ORIGINAL RESEARCH REPORT

The influence of structure and morphology on ion permeation in commercial silicone hydrogel contact lenses

Virginia Saez-Martinez[1] | Aisling Mann[1] ⬤ | Fiona Lydon[1] | Frank Molock[1] |
Siân A. Layton[1] | Daniel T. W. Toolan[2] | Jonathan R. Howse[3] |
Paul D. Topham[4] ⬤ | Brian J. Tighe[1]

[1]Biomaterials Research Unit, Chemical Engineering and Applied Chemistry, Aston University, Birmingham, UK

[2]Department of Chemistry, University of Sheffield, Sheffield, UK

[3]Department of Chemical and Biological Engineering, University of Sheffield, Sheffield, UK

[4]Aston Institute of Materials Research (AIMR), Chemical Engineering and Applied Chemistry, Aston University, Birmingham, UK

Correspondence
Aisling Mann, Biomaterials Research Unit, Chemical Engineering and Applied Chemistry, Aston University, Birmingham, B4 7ET, UK.
Email: a.m.mann@aston.ac.uk

Present address
Virginia Saez-Martinez, i+Med, Vitoria-Gasteiz, Spain

Abstract

The importance of the microstzructure of silicone hydrogels is widely appreciated but is poorly understood and minimally investigated. To ensure comfort and eye health, these materials must simultaneously exhibit both high oxygen and high water permeability. In contrast with most conventional hydrogels, the water content and water structuring within silicone hydrogels cannot be solely used to predict permeability. The materials achieve these opposing requirements based on a composite of nanoscale domains of oxygen-permeable (silicone) and water-permeable hydrophilic components. This study correlated characteristic ion permeation coefficients of a selection of commercially available silicone hydrogel contact lenses with their morphological structure and chemical composition. Differential scanning calorimetry measured the water structuring properties through subdivision of the freezing water component into polymer-associated water (loosely bound to the polymer matrix) and ice-like water (unimpeded with a melting point close to that of pure water). Small-angle x-ray scattering, and environmental scanning electron microscopy techniques were used to investigate the structural morphology of the materials over a range of length scales. Significant, and previously unrecognized, differences in morphology between individual materials at nanometer length scales were determined; this will aid the design and performance of the next generation of ocular biomaterials, capable of maintaining ocular homeostasis.

KEYWORDS

contact lens, ESEM, ion permeation, SAXS, silicone hydrogels

1 | INTRODUCTION

The design of a contact lens material should not seek merely to create a bio-inert temporary implant, but preferably it should be capable of maintaining the existing homeostasis of the avascular corneal bed in equilibrium with its external environment. However, currently no single material exhibits the required ocular biocompatibility to enable asymptomatic long-term use and good ocular comfort across a wide patient base. The most common symptoms that are associated with elective discontinuation of wear are discomfort and dryness.[1-3] The goal for any new contact lens is that it should allow a suitable balance of oxygen and ion permeability, appropriate on-eye movement, and
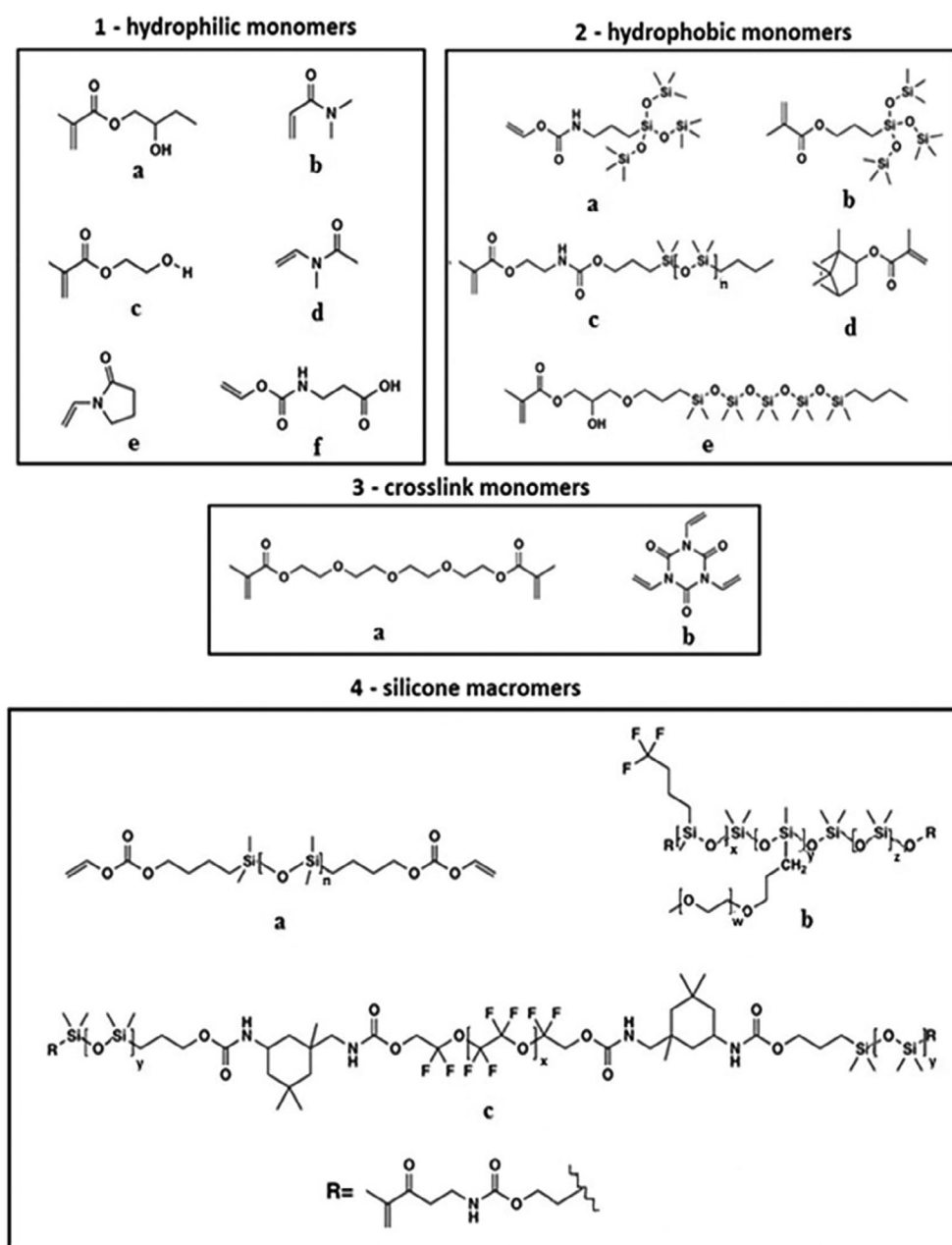
satisfactory tear exchange. Lens permeability is critical in enabling the free movement of nutrients, the removal of metabolic waste products, and the dynamic distribution of tear film components including water, electrolytes, and proteins to maintain ocular homeostasis.[4,5]

Early soft contact lenses were based on poly(2-hydroxyethyl methacrylate) (pHEMA) hydrogels. These, although well hydrated, soft, and relatively comfortable, fell well short of providing the degree of oxygen permeability needed to facilitate corneal cell homeostasis.[6,7] Consequently, there has been a progressive evolution of contact lens materials from conventional hydrogels to more oxygen permeable silicone hydrogel (SiHy) materials. The oxygen permeability of commercial SiHys is known to be high.[8] As contact lens technology has evolved, recognition of the desirability of maintaining a pre- and post-lens tear film that mimics the natural tear film (which has a

distinct electrolyte composition) has become clear.[9-12] The permeation of tear electrolytes is, however, much more variable and at the heart of this study, as reported previously ion permeation does not show a uniformly predictable dependence either on equilibrium water content (EWC) alone or the water structuring within the material.[13] According to Domschke et al., ion permeability within contact lenses is a critical parameter for lens movement on the eye[4] and it is also thought to be a requirement for post-lens tear turnover and metabolic waste removal.[12] Similarly, the electrolyte composition of tears, which is quite distinct from that of serum, can be adversely affected by the presence of a barrier, which disturbs ion transport creating a post-lens tear film.[7] In addition, studies involving more detailed clinical-based analysis have shown that different materials can affect physiochemical properties which in turn can influence the nature and composition of

FIGURE 1 Monomer chemical structures for the four silicone hydrogels. (1a) HBMA; (1b) DMA; (1c) HEMA; (1d) VMA; (1e) NVP; (1f) NCVE; (2a) TPVC; (2b) TRIS; (2c) PBVC; (2d) IBMA; (2e) SiHPMA; (3a) TEGDMA; (3b) TAIC; (4a) SM1; (4b) SM2; (4c) SM3 (see Table 1 for full monomer names)

the post-lens tear.[14-16] Differences in the occurrence of corneal infiltrative events have been identified between commercial SiHys[17]; materials that have similar high oxygen permeabilities but very different ion permeabilities.[13,18]

The influence of polymer phase morphology, which can take many forms, on lens movement on the eye has been highlighted.[19] Structure–property–performance relationships are important. Identification of the causative factors that link physicochemical properties, disturbance of corneal homeostasis, and long-term ocular biocompatibility does, however, remain elusive. A more comprehensive understanding of the relationships between physicochemical properties and the underlying SiHy structure needs to be established. All SiHy materials are a subset of a larger group of materials that can be defined as hydrophobically modified hydrogels. The chemical nature of the selected monomers and the ratios in which they are employed can have a profound effect on the nanoscale structure within the material. This, in turn, plays a huge role in determining the final physical properties displayed by the material.[20-22] A range of siloxy monomers and macromonomers is used in the preparation of SiHys, typically combined with other, more hydrophilic, monomers (Figure 1; Table 1). Siloxy and hydrogel-forming monomers are clear, low refractive index (RI) materials with values close to ~1.5.[23] In combination with water (RI = 1.33), phase separated regions can generate haze, translucence, and opacity—dependent on domain size. The hydrophobic nature of silicones means that they have a marked tendency to phase-separate in aqueous systems. Successful design of silicone monomer precursors

for SiHy fabrication entails the incorporation of sufficient hydrophilic motifs as part of the monomer to provide compatibility with conventional hydrogel-forming monomers (such as pHEMA, N-vinyl pyrrolidone [NVP], or N,N-dimethylacrylamide [DMA]). The siloxy groups are either enchained within macromonomers (typically containing ethylene oxide units to enhance hydrophilicity) or incorporated as linear or branched pendant groups (Figure 1, part 4).

The primary consideration of manufacturers, in selecting combinations and ratios of these monomers, is to ensure that nanoscale separation and self-assembly of the siloxy units does not extend so as to impair the optical clarity of the final water-swollen SiHy network; an obvious requirement for ophthalmic use. The extent of separation and self-assembly of the siloxy groups is limited by the degree of mobility afforded during the polymerization (chain growth, branching, and crosslinking) process. The final nanoscale domain structure is therefore controlled by both composition and polymerization process. The use of diluents (Table 2) provides another degree of control in the development of haze-free, optically clear contact lens materials by producing an appropriate balance between the various constituents.[28]

Despite significant progress in understanding the basic structure–property relationships of networks, much remains to be learned about how the foundational macromolecular building blocks influence structure from the nano to the macroscopic scale. In this study, four commercial SiHy materials were selected. They enable the study of SiHys with similar water contents but very different ion permeation properties as previously shown by Mann et al.[13] Two of the chosen materials have relatively high quoted EWCs: narafilcon A (44%) and comfilcon A (48%), and two have lower water contents: lotrafilcon B and balafilcon A (both 34%). To investigate factors that may influence the disparate ion permeability properties of each material, the structural morphology at different length scales of each of these four materials was investigated by environmental scanning electron microscopy (ESEM) and small angle x-ray scattering (SAXS) together with specific water structuring properties of each lens material.

2 | MATERIALS AND METHODS

The properties and components of four commercial SiHys namely narafilcon A, comfilcon A, lotrafilcon B, and balafilcon A which were selected based on their water content and ion permeation properties[13] are shown in Table 2.

2.1 | Differential scanning calorimeter (DSC) analysis

Differential Scanning Calorrimetery (DSC7 with hypercooler, Perkin Elmer, London, UK) was used to measure the hydration and water binding characteristics of lenses in packing solution, pure DI water (with a resistivity of 18.2 MΩ·cm [Purite Ltd., Oxon, UK]), and after permeation studies ($n \geq 3$). Surface water was removed from the lens with filter paper and the samples were weighed and then hermetically

TABLE 1 Silicone hydrogel constituents and abbreviations

Chemical	Abbreviation
2-hydroxybutyl methacrylate	HBMA
N,N-dimethylacrylamide	DMA
2-hydroxyethyl methacrylate	HEMA
N-methyl-N-vinylacetamide	VMA
1-vinylpyrrolidin-2-one	NVP
3-(((vinyloxy)carbonyl)amino)propanoic acid	NCVE
Vinyl (3-(1,1,1,5,5,5-hexamethyl-3 ((trimethylsilyl)oxy)trisiloxan-3-yl)propyl)carbamate	TPVC
3-(1,1,1,5,5,5-hexamethyl-3-((trimethylsilyl) oxy)trisiloxan-3-yl)propyl methacrylate	TRIS
2-(((3-(3-butyl-1,1,3,3-tetramethyldisiloxaneyl) propoxy)carbonyl)amino)ethyl methacrylate	PBVC
Isobornyl methacrylate	IBMA
3-(3-(9-butyl-1,1,3,3,5,5,7,9,9-decamethylpentasiloxaneyl)propoxy)-2-hydroxypropyl methacrylate	SiHPMA
Triethylene glycol dimethacrylate	TEGDMA
1,3,5-trivinyl-1,3,5-triazinane-2,4,6-trione	TAIC
(1,1,3,3-tetramethyldisiloxane-1,3-diyl) bis(butane-4,1-diyl) divinyl bis(carbonate)	SM1
Representative structure derived from patents	SM2
Representative structure derived from patents	SM3

TABLE 2 Silicone hydrogel contact lens properties, permeation coefficients and components (see Figure 1 for component structures)

United States adopted name	Balafilcon A	Comfilcon A	Lotrafilcon B	Narafilcon A
Name	PureVision	Biofinity	O_2 Optix	Acuvue TruEye
Manufacturer	Bausch & Lomb	CooperVision	Alcon	Johnson & Johnson
EWC (%)[a]	34.2 ± 0.6	47.5 ± 0.5	34.4 ± 0.9	44.2 ± 0.4
Dk (barrers)[b]	99	128	110	100
KCl permeation coefficient[c]	258 ± 38	228 ± 16	136 ± 4	3.9 ± 1.4
NaCl permeation coefficient[c]	225 ± 6	186 ± 11	89 ± 4	3.7 ± 2.7
$CaCl_2$ permeation coefficient[c]	175 ± 16	166 ± 15	70 ± 20	0.5 ± 3.4
Hydrophilic monomers	NVP, NCVE	HBMA, DMA, VMA	DMA, HEMA	DMA, HEMA
Hydrophobic monomers	TPVC	TRIS, PBVC, IBMA	TRIS	SiHPMA
Crosslinkers	n/d	TAIC	n/d	TEGDMA
Silicone macromers	SM1	SM2	SM3	—
Diluents[24-27]	Isopropanol, n-hexanol	n/d	Neopentyl alcohol, ethanol	Decanoic acid, tripropylene glycol monomethyl ether

Abbreviation: n/d, not disclosed.
[a]Measured in water after a 7 day pre-soak in deionized water.
[b]$Dk \times 10^{-11}$ (cm^2/s) $(mlO_2/ml \times mmHg)$ @34–35°C measured in packing solution.
[c]$P_{(60)} \times 10^8$ (cm^2/s) at initial rate P60 mins.[5]

sealed in aluminum sample pans. Samples were scanned from −50 to 25°C with a heating rate of 5°C/min. The software enables calculation of the area under the melting (endotherm) peak and the quantification of the energy associated with phase change, in J/g. Using this information and dividing by the heat of fusion of pure water (79.72 cal/g = 333.55 J/g) then multiplying by 100 allows the percentage of free or freezing water to be calculated. The total area under the endotherm peak corresponds to the total freezing water content (FWC), which is the sum of the ice-like water content (ILWC) and the polymer-associated water content (PAWC), illustrated previously.[13] The non-freezing water content (NFWC) was calculated by subtraction of total freezing water from the measured EWC. All values are expressed as percentages of the total mass of the hydrated lens.

2.2 | Environmental scanning electron microscopy (ESEM)

The topography and heterogeneities of the SiHy contact lenses were observed with a Philips XL30 FEG (Thermo Fisher Scientific, Waltham, MA) ESEM equipped with a cold stage. Each hydrated lens was prepared for mounting as shown in Figure 2 to image the cross-sectional surface. The lenses were prepared using a colloidal carbon mount. They were rapidly immersed at −180°C for 1 min and sublimated at −95°C for 5 min. Samples were then transferred into a PolarPrep 2000 cryo-stage system chamber enabling rapidly frozen samples to be analyzed at −140°C. The accelerating voltage was set at 5 kV, with a working distance range of 3 to 5 mm. The samples were analyzed at ×35,000 magnification. The system was set to detect secondary electrons used for sample surface topography.

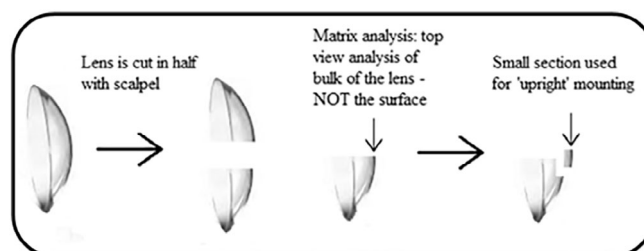$2D34689\text{-}FIG\text{-}0002\text{-}b''$

FIGURE 2 Contact lens sectioning for environmental scanning electron microscopy analysis

The heterogeneity of each image suggests discontinuities in the physical topographical structure of each material. Using five individual lens matrix section images—which are consistently characteristic of each material—the percentage of what we have termed "apparent porosity" (black vs. white) of the materials was determined. In principle, the lower the mean atomic number of a sample under a beam, the fewer electrons are generated/detected and the resultant pixel for that region will consequently be dark. Thus, a pore or void, which is atomically light, will always appear dark if it is adjacent to an atomically heavier polymer region. Each image was assessed by using the Java-based image processing program ImageJ.[29] After adjusting the initial threshold, the ImageJ plugin for particle analysis was used.

Cluster sizes were measured taking an average of 20 visually similar domain sizes on five separate images. The software was also used to calculate the "apparent porosity" (white) by subtracting the region occupied by the polymer clusters (black) from the total area of each image, a threshold between 75 and 95% was used, accounting the vagaries of the microscopy image capture settings, images were obtained of the internal region of the material and not the surfaces of the lens.

In SEM, the returned signal is provided by the amount of material in the path length of the electron beam. In our samples, where there are deep crevasses or voids, the returned signal is less intense (less material in the beam path) and therefore appears dark. In contrast, the areas where there is ample polymer in the beam path appear brighter (more material = higher intensity). In short, these allow the topology of the material to be mapped out and give an impression of the surface porosity.

2.3 | Small angle x-ray scattering (SAXS)

SAXS, a nondestructive x-ray technique, was used to investigate particle size, shape distribution, and morphology at the nanoscale level. Measurements were conducted on a laboratory SAXS instrument (Xeuss 2.0, Xenocs, France) equipped with a liquid gallium MetalJet X-ray source (Excillum, Sweden), wavelength (λ) = 0.134 nm, beam size approximately 2 mm^2, camera length = 2.4 m (calibrated using a silver behenate standard) and Dectris Pilatus 1 M pixel detector. Samples (ca. 100 μm thickness) were placed in a cell (1.5 mm depth) with deionized water and sealed with Kapton®. Scattering data were collected for 900 s using collimating slits of 0.5×0.6 mm ("high flux" mode). The scattered x-rays were adjusted for transmission, background (water and Kapton®), sample thickness, and acquisition time before the intensity data were placed on an absolute scale (cm^{-1}) using scattering from a standard sample of glassy carbon.[30] Data reduction from a 2D scattering pattern to 1D intensities as a function of q (scattering vector, nm^{-1}) was performed using the instrument-specific Foxtrot software and custom LabView code. Spacing between domains was calculated using the following equation: $d = 2\pi/q$, where the q values of each lens were taken from the first major feature of the corresponding radially integrated scattering pattern.

2.4 | Statistical methods

Descriptive statistics in terms of mean and standard deviation are provided, Figure 4 where $n \geq 3$ and in Figure 6 they denote the variation for five separate images on each lens material. Figure 7 shows normalized 1D data where Foxtrot (Xuess in-built software) estimates the statistical error on the intensity counts and propagates it (via propagation of the Poisson statistics from the two-dimensional variation of counts from the Pilatus detector) while performing the radial integrals when reducing 2D scattering data to 1D.
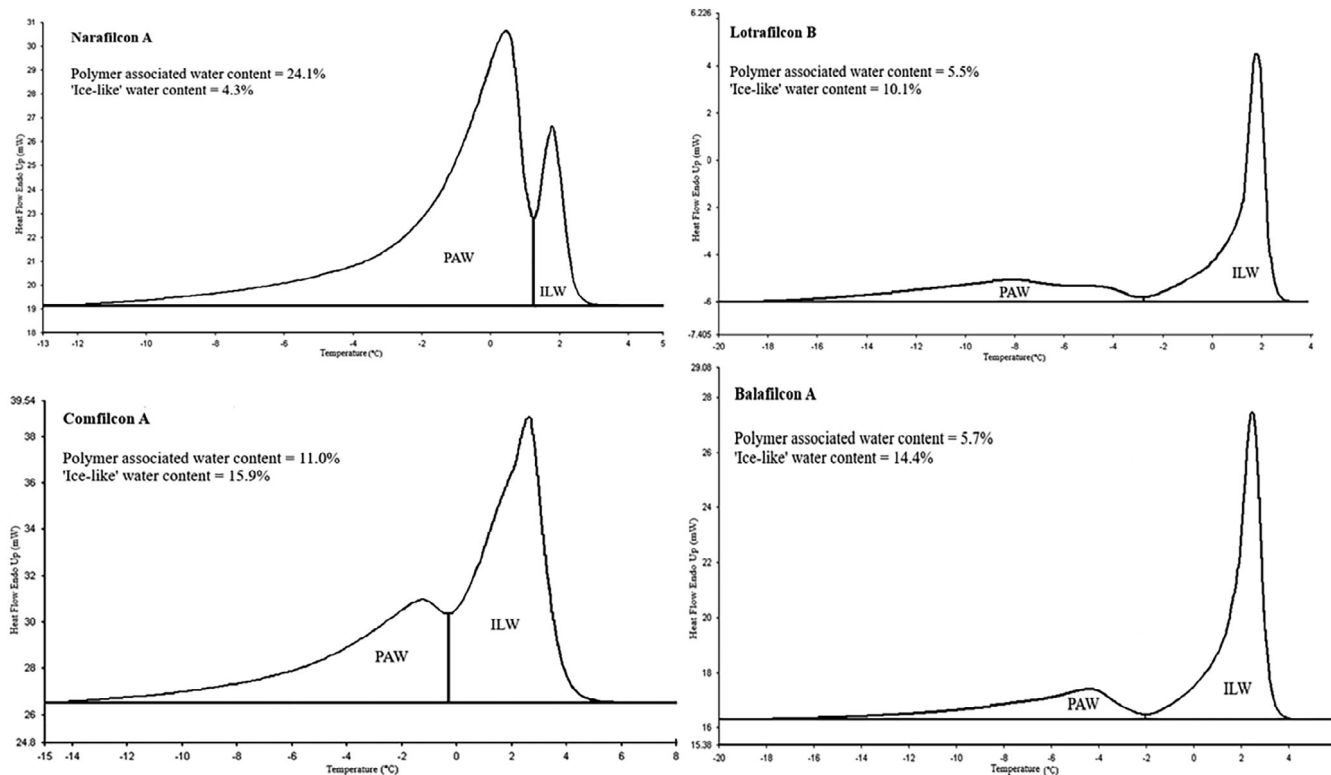

FIGURE 3 Typical DSC traces for narafilcon A, lotrafilcon B, comfilcon A, and balafilcon A, illustrating the percentages of polymer associated and "ice-like" water

3 | RESULTS

3.1 | Water structuring

Table 3 summarizes the hydration properties of the lenses after a 7-day hydration in deionized water before ion permeation. One representative DSC trace showing the water structuring profile for each of the four materials is provided in Figure 3. The difference between FWC (= PAWC + ILWC) and total EWC indicates that all contact lenses have approximately 15 to 20% nonfreezing water of the total lens weight. It is the distribution of freezing water between ILWC and
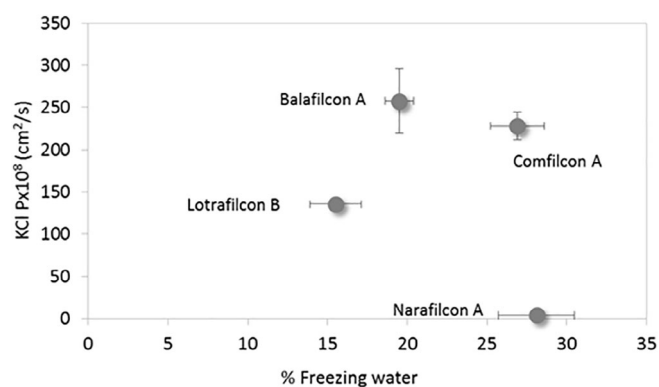

FIGURE 4 Mean (±*SD*) KCl permeation coefficients (Px10^{8}cm^2/s) for lotrafilcon B, balafilcon A, narafilcon A, and comfilcon A compared with their respective freezing water percentages (*n* = 3)

PAWC (Section 2.2) that is of interest here, since this is critical for the interaction of hydrated ions with water within the polymer matrix. Water structuring values for lenses in packing solution, DI water, and post ion permeation showed slight differences for each condition but these lay within standard deviations (e.g., FWC for comfilcon A in packing solution, DI water, and post NaCl permeation were 27.9 ± 0.6, 26.9 ± 1.7, and 26.1 ± 1.9%). Water structuring results discussed here and thereafter refer to those measured in DI water to represent the ion permeation analysis conditions. Narafilcon A material was observed to contain uniquely high values of polymer-associated water (23.7 ± 2.1%) compared to a very low ice-like water content (4.4 ± 0.4%). In contrast and at the other extreme, the level of ice-like water within comfilcon A was higher (16.6 ± 1.6%) than that of polymer-associated water (10.4 ± 0.7%). Balafilcon A also shows a higher ratio of ice-like (13.9 ± 0.6%) compared to polymer-associated water (5.6 ± 0.3%), although in balafilcon A the total water content is significantly lower than that of comfilcon A (34.2% compared to 47.5%). Lotrafilcon B has the same EWC as balafilcon A, a similar amount of polymer-associated water (5.2 ± 0.8%), but less ice-like water (10.3 ± 0.9%).

Unlike conventional hydrogels,[31] no clear relationship between FWC and ion permeability was observed. This can be seen with the KCl permeant as an example (Figure 4). The lack of correlation with either FWC or EWC and ion permeation is clear. Although there are broad structural similarities between the four materials there may well be significant differences in the self-assembly characteristics of silicone segments with these complex monomer mixtures (Figure 1; Table 2). It was therefore logical to investigate differences in physical
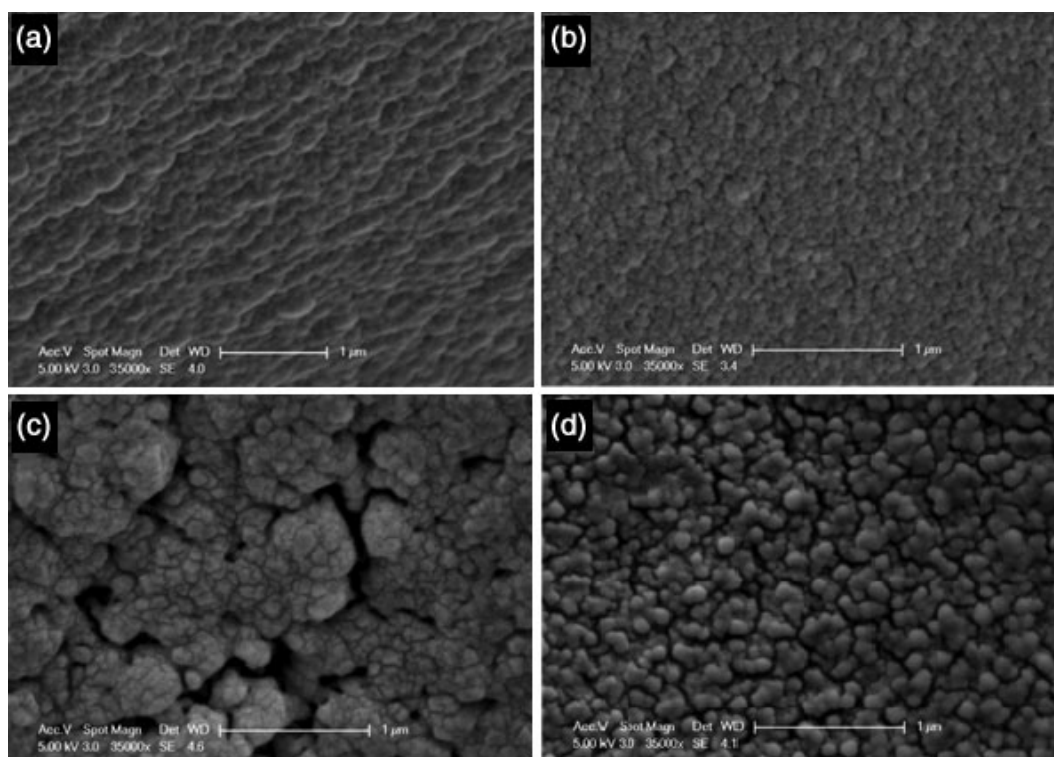

FIGURE 5 ESEM images of the hydrated lenses (a) narafilcon A, (b) lotrafilcon B, (c) comfilcon A, and (d) balafilcon A. Scale bar = 1 μm
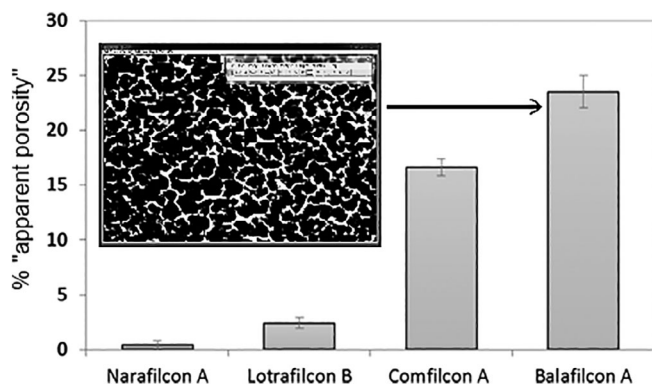
FIGURE 6 Percentage "apparent porosity" of bulk materials estimated by ImageJ from the ESEM images of the four commercial contact lenses. Inset: example of an image of balafilcon A processed by ImageJ

FIGURE 7 1D SAXS data for the balafilcon A, comflicon A, lotrafilcon B, and narafilcon A silicone hydrogel contact lenses, taken from radially integrated 2D scattering patterns. The inset shows the data without error bars for clarity purposes. Approximate q-values (and corresponding length scales) of the first major feature in each scattering pattern have been indicated

morphology and their possible links to levels of polymer-associated and ice-like water since inspection of the data suggests that these characteristics are more influential than either EWC or FWC in governing ion permeability.

3.2 | ESEM imaging of the matrix of the SiHy contact lens materials

Characteristic structures were observed for all samples (Figure 5), suggesting a degree of heterogeneity more marked in comfilcon A and balafilcon A than in narafilcon A and lotrafilcon B. The "apparent porosity" was analyzed using the ImageJ software, and calculated as a percentage of the total image in each case at a magnification of ×35,000 (n = 5), as illustrated in the insert in Figure 6. The least ion permeable material, narafilcon A, showed the lowest percentage of "apparent porosity" while the most ion permeable material, balafilcon A, exhibited the highest percentage (Figure 6). Cluster size population averages for the lens materials are summarized in Table 4. Visual inspection of porosity and cluster size by the ImageJ suggest that narafilcon A, the least ion permeable material, showed the lowest porosity and higher polydispersity of sizes, which has three different populations. The more porous materials, comfilcon A and balafilcon A, show larger and more uniform domain populations (Table 4).

3.3 | Internal nanostructure assessment by small angle x-ray scattering

SAXS has been shown to be a very powerful technique for providing insight into nanoscale morphological features for a wide variety of systems.[32-36] In SAXS measurements, contrast between two components increases in proportion to the square of the electron density difference. As such, for all samples studied herein, any peaks in the SAXS scattering data will arise from populations of the more electron dense component (Si rich hydrophobic components), spatial separated by
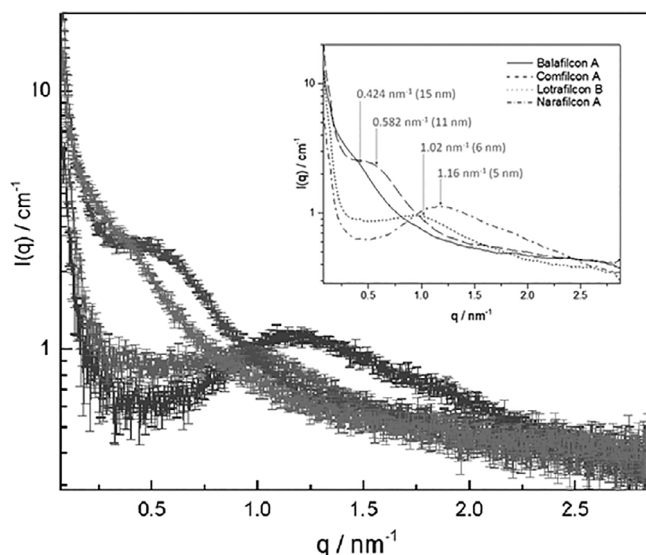
TABLE 3 Mean (±SD) measured equilibrium water contents (EWC), polymer-associated water contents (PAWC), ice-like water contents (ILWC), and non-freezing water contents (NFWC) ($n \geq 3$). Materials are listed in order of increasing permeability

	Water structuring data (%)[a]			
Contact lens	**EWC**	**PAWC**	**ILWC**	**NFWC**
Narafilcon A	44.2 ± 0.4	23.7 ± 2.1	4.4 ± 0.4	16.1 ± 1.3
Lotrafilcon B	34.4 ± 0.9	5.2 ± 0.8	10.3 ± 0.9	18.9 ± 1.6
Comfilcon A	47.5 ± 0.5	10.4 ± 0.7	16.6 ± 1.6	20.5 ± 1.7
Balafilcon A	34.2 ± 0.6	5.6 ± 0.3	13.9 ± 0.6	14.7 ± 0.9

[a]Measured after a 7 day DI water pre-soak.

the less electron dense components, the hydrophilic components. For these complex, multicomponent systems, SAXS data exhibiting no peaks would be consistent with mixing of both the hydrophobic and hydrophilic components. Although the reciprocal length scale of any scattering arises as a consequence of distinct regions of electron density, peak broadening could be attributed to both the size distribution of such domains and also their purity. Radially integrated SAXS data for the hydrated comfilcon A, balafilcon A, lotrafilcon B, and narafilcon A contact lenses are presented in Figure 7, with each exhibiting scattering features in the region between q = 0.3 and 2.0 nm^{-1}. The SAXS data indicate that there are significant differences in the nanoscale morphologies for the four different SiHy contact lenses studied here. The approximate q-value and corresponding d-spacing of the first major feature in each scattering pattern (Figure 7) provide information on the length scale of the self-assembled domains. It should be noted

that the SiHy systems studied here do not possess highly ordered, well-defined nanoscale morphologies as observed previously,[37] where Seitz et al., showed purpose-synthesized silicone-based copolymers formed morphologies consisting of core-shell spheres, dispersed with liquid-like order. It is not surprising that the commercial SiHy contact lenses studied here do not form such well-defined nanomorphologies, owing to increased formulation complexity (shown in Table 2; Figure 5). Likewise, it is important to note that SAXS tells us about the dominant length scale within the material but not necessarily the interconnected nature of these domains. SAXS measures self-assembled domains in our samples (5–50 nm length scale) whereas ESEM is measuring surface topology area in the region of 50 nm – 100 μm.

4 | DISCUSSION

4.1 | Ion permeation behavior and water structure

The differences in the behavior of a series of commercial SiHy materials of apparently similar chemical structure (Figure 1; Table 2) were examined using hydrated cations as molecular-level probes. Despite the many apparent similarities (e.g., optical clarity, oxygen permeability, and tensile modulus), the materials differ dramatically in other ways, particularly ion permeability (Table 2). Ion permeability in conventional hydrogels is known to be governed simply by water content and water structure, the picture for SiHys is more complex, a point underlined by the huge differences in ion permeabilities found with SiHys of similar water content.[13] In seeking an explanation for the unusual ion transport behavior of SiHys, it is logical to explore the way that differences in the self-assembly characteristics of siloxy moieties leads to complex morphologies in SiHys. These are not found in their conventional hydrogel counterparts and may well reveal unexplored characteristics of this group of materials.

Balafilcon A and comfilcon A have been shown to exhibit the highest ion permeation rates, followed by lotrafilcon A, and then narafilcon A, by far the least ion-permeable material of this group. Potassium permeation values were higher than those for sodium, which in turn were higher than calcium.[13] Relative permeation values of the individual ions were observed to agree with the Stokes' (or hydrodynamic) radii and the relative ionic mobilities, which increase in the order $K^+ < Na^+ < Ca^{2+}$ (Table 5). Table 5 also shows the hydrodynamic

TABLE 4 Average diameter distribution of the contact lenses microstructure clusters analyzed from the ESEM images with the ImageJ software

Domain size	Small (nm)	Large (nm)
Lotrafilcon B	63 ± 7	99 ± 16
Narafilcon A	62 ± 8	89 ± 11
	—	111 ± 17
Comfilcon A	67 ± 10	116 ± 15
Balafilcon A	—	99 ± 12

radius of the chloride counter-anion which, importantly, does not have a rate-determining role.[31] The differences observed in the initial profile, shape, and slope of the curves shown previously[13] reflect differences in the way that the various material structures and charges interact with the aqueous salt solutions and with water in affecting transport through the matrix. From inspection of Table 3 and Figure 4, the broad correlations between the ion permeation values and EWC or FWC found in simpler hydrogel systems[31] and even proposed for SiHys[18] have broken down here. This is highlighted by the relative behavior of narafilcon A and balafilcon A and emphasizes the relevance of understanding compositional and morphological effects on the transport behavior of this important class of ophthalmic biomaterials.

DSC studies have provided some significant insight into the effects of the polymer matrix on water structure, in particular the splitting of the melting endotherm associated with the water in the hydrogel matrix that is able to freeze. The endotherm splits conveniently into "ice-like" water and water with a depressed melting point (characterized as "polymer-associated" water). To understand these observations, a basic understanding of the unique behavior of water is required. The structure of water (four electron pairs on four sp^3 orbitals, two pairs of which covalently link hydrogen atoms to a central oxygen atom, whereas the two remaining pairs remain as nonbonding lone pairs) means that it can serve as both a hydrogen bond donor and acceptor and thereby exhibits a unique tetrahedral structure. Whereas in ice each water molecule forms four hydrogen bonds, in liquid water, each water molecule forms on average 3.4 hydrogen bonds. Ions can polarize water and become solvated by it, although this disrupts the tetrahedral structure of water, disturbance is generally relatively minimal (depending on the size and charge of the ion).[41,42]

Disruption and "ordering" of hydrogen bonded water networks is greater near a hydrophobic solute. Water hydrates the hydrophilic portion of amphiphiles but excludes the hydrophobic regions to yield (e.g.,) micelles and lipid bilayers, thereby reducing entropy in thermodynamically driven processes. Extending these principles to optically clear hydrophobically modified hydrogels, the nature of "polymer-associated" water becomes clearer. Disruption and reordering of the tetrahedral structure of water is induced by even modestly hydrophobic polymer chains with consequent deviation from perfect ice networks on freezing, which has an inevitable effect on melting behavior. If the polymer chains are clustered to form pores, the proportion of "ice-like" to "polymer-associated" water increases. This can be seen here in the higher proportions of ice-like water in the more porous comfilcon A and balafilcon A matrices.

The free mobility of hydrated ions through an aqueous matrix inevitably requires the ability of the hydrated ion to exchange water molecules with the surrounding medium. It is logical to expect that hydration phenomena related to this will influence ion permeation behavior in SiHys. It was observed that narafilcon A was found to have both low permeability characteristics and much lower ice-like water than the other three materials studied. In simplistic terms this means that there is very little available water with the ability to

TABLE 5 Crystal ionic radius, hydrodynamic radius and diffusion coefficient of the ions used in this study[38-40]

Ion	Crystal radius (Å)	Hydrodynamic radius (Å)	Diffusion coefficient (10^{-9} m^2/s)
Na$^+$	1.16	3.58	1.334
K$^+$	1.52	3.31	1.957
Ca^{2+}	1.14	4.12	0.792
Cl$^-$	1.67	3.32	2.032

FIGURE 8 Sodium chloride permeation values, "apparent porosity" obtained from ESEM images and d-spacing obtained by SAXS, of the four different contact lenses analyzed. Sodium chloride has been selected here as a representative for the salts, which all follow a similar trend

hydrate cations and sustain their freedom of movement within the polymer network. It is clear, however, that results from water freezing analysis and the ratios of bound and free water alone do not provide a complete explanation of the ion permeation properties demonstrated by these materials, unlike conventional pHEMA-based contact lenses.[13] The phase separated nanostructure in SiHys, reflected in the SAXS results, and the mesostructures as observed by ESEM will also affect their ion permeation behavior.

4.2 | Composition, morphology, and internal nanostructure

It has been postulated that the existence of two separate phases in SiHy materials, rather than a single homogeneous phase, may be advantageous, promoting both the diffusion of ions through the hydrophilic regions of the polymer (so-called hydration channels), and increased diffusion for oxygen through the silicone-rich regions.[24] Although the hydrophilic regions of the material provide good diffusion of ions, they provide a relatively high barrier to oxygen diffusion.[24] An excellent discussion of the evolution of contact lens morphologies and the concept of independent control of oxygen and ion transport by means of co-continuous morphologies reflects aspects of the commercial knowledge that has been amassed in recent years.[19]

The ESEM images provide good quality imaging of hydrated samples allowing better visualization of structures at the mesoscale, showing clear differences between each of the materials. The calculated apparent porosity corresponds to two different types of structure: homogeneous small scale closed structures (narafilcon B and lotrafilcon A) and higher aggregated blocks with interconnected pores and channels (balafilcon A and comfilcon A). The calculated and measured permeabilities showed good agreement with this observation. Channeled structures organized in the repetitive manner of balafilcon A and comfilcon A, support a hypothesis linking mesostructured porosity to the ion permeability of these materials. Thus, the ion permeation coefficient increases with the increased "apparent porosity" determined by image analysis of each sample. A weaker correlation between ice-like water contents and the permeation of salts through these SiHys was observed, whereas there seems to be no correlation between the EWC (which takes into account bound water) and ion permeation. It is interesting to note that balafilcon A has less ice-like
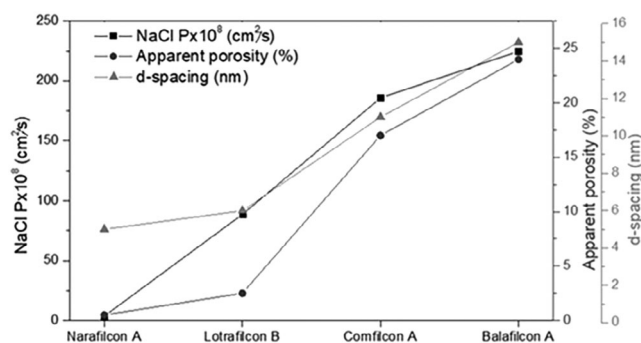
water than comfilcon A, but a higher permeation coefficient for each salt studied in this work. However, balaficon A has a higher percentage of "apparent porosity" (Figure 6) and greater visually assessed interconnectivity between the heterogeneities observed in Figure 5. This appears to allow increased diffusion of salts through the material. The samples with lower "apparent porosity": narafilcon A and lotrafilcon B, show much smaller nanoscale cluster sizes (as measured by SAXS), and have the lowest values of permeation coefficient for all salts studied here.

The data suggest that materials with a relatively large interconnected mesoporous structure lead to higher ion permeabilities. SAXS was used to probe smaller length scales than ESEM, that is, the internal nanostructure of the lens material. Previous results have indicated a nanophase separated structure of silicone rich (oxygen permeable) and hydrophilic (water soluble) polymer domains separated on a length scale of about 10 nm.[43,44] Notably, it was observed that the self-assembling nature of hydrophobic silicone-based domains gave rise to varying degrees of order on the nanoscale. In our work, each contact lens gave a different scattering pattern over the q-range studied, indicative of varying order and domain spacing on the nanoscale. From the SAXS data, it was clear that larger self-assembled domains are observed for balafilcon A (albeit in the most weakly ordered system in the series), followed by comfilcon A, and then lotrafilcon B. Narafilcon A has the smallest self-assembled domains, suggesting a much tighter network of clusters. Domain spacing deduced from SAXS analysis follows the same trend as the apparent heterogeneities observed in the ESEM images. The samples with smaller nanoscale features, as revealed in SAXS, show more compact, less open structures in the mesoscale morphology shown in ESEM. Interestingly, these hydrogels have decreased salt permeation through their networks.

The correlation between structure and ion permeability can be seen more clearly in Figure 8 (which is assembled merely for convenient comparison; statistical reliability data are presented in the experimental and results sections), where the different trends obtained by the different techniques are presented for comparison. These data
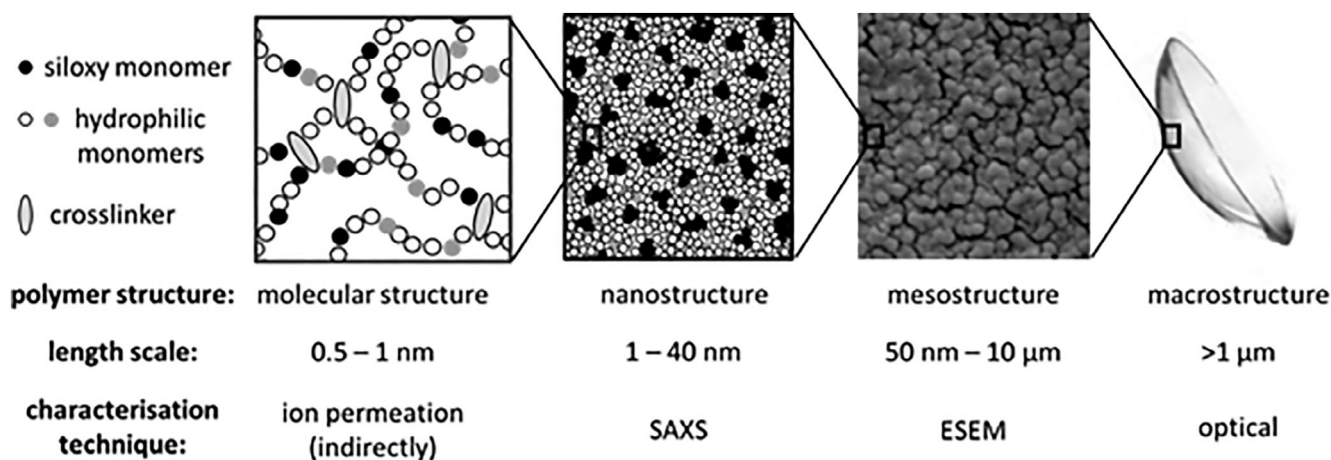
FIGURE 9 Schematic of the various structural length scales of the contact lenses, starting with the molecular composition of the polymer chains (left) to the bulk contact lens itself (right). The cartoon sketches of the polymer chains and the internal nanostructure are for illustrative purposes and are not intended to be an accurate structural portrayal

suggest that there is a correlation between the features at the nanoscale and the ion permeability of the material. It is also important to note that there is strong correlation between size of the nanostructures (on the order ∼10 nm) and the heterogeneous mesostructures (on the order of ∼200–500 nm), suggesting that a more diffuse system (weaker phase separation with concomitant increase in distance between hydrophobic clusters) delivers a potentially more porous structure, which gives rise to increased ion permeability. This work demonstrates the importance of characterization techniques that are capable of probing the nano- and mesostructures of silicone-based hydrogels, where simple design rules based solely on water content cannot be used to predict the ion permeability behavior of the material, unlike in conventional pHEMA-based hydrogels.

There are many examples of the use of induced porosity in biomedical applications of polymers. These are common in the micron range and readily studied by conventional scanning electron microscopy.[45,46] Based on the findings here, the heterogeneities that appear to link to porosities found in commercial SiHys occur at much lower length scales (as summarized in Figure 8), and appear to be adventitious consequences of siloxy self-assembly processes, rather than the result of intentional design. They do, however, have significant consequences for the ion permeation behavior of the resultant materials.

Although the two-dimensional ESEM images cannot represent a direct measure of three-dimensional interconnected pores, the data are consistent and should not therefore simply be discarded. The obvious concurrence of different measurement techniques (Figure 8) indicates that image heterogeneity does reflect a phenomenon that directly influences transport behavior. Another aspect of this study that remains elusive is the direct correlation of the chemistry of the siloxy precursors and overall composition of the SiHy materials (Figure 1; Tables 1 and 2) with the resultant differences in morphology; this in part is due to the lack of precise compositional information. The patent literature, together with regulatory submissions, has enabled the compiled information shown here to be assembled. This provides a useful basis for some general observations and conclusions.

In contrast, the "apparent heterogeneities" observed here occur at much shorter length scales than those influencing optical clarity (ca 500 nm) and require sophisticated investigative instrumentation—in the domain of molecular self-assembly—driven by the fundamental incompatibility of silicone moieties and water.[8,21]

The driving principles in the design of SiHys with optical clarity have been to combine siloxy groups (e.g., TRIS, Figure 1, structure 2b) with hydrophilic monomers, compatibilizing macromers, and diluents designed to maintain compatibility during the lens processing stage. The material with the least "apparent heterogeneity" is narafilcon A. The SiHPMA structure (Figure 1, structure 2e) has a hydroxyl ester moiety in close proximity to a relatively short siloxy chain containing five silicon atoms. Of all the SiHy material structures, this presents the least opportunity for self-assembled siloxy units that exclude covalently bonded hydrophilic groups. This material clearly has the lowest degree of "apparent porosity" (Figures 5 and 6). The description of the design considerations that accompanied the development of lotrafilcon A is contained in an extensive patent application.[24] This places great stress on the development of appropriate macromer structures, which dominate the formulation, typified by Figure 1, structure 4c. This is characterized by relatively short linear siloxy segments interspersed with fluoroether units. As with narafilcon A, the hydrophilic "solvent-monomers" are N,N-dimethyl acrylamide (NNDMA) and HEMA (Table 1; Figure 1). Without comparative data, no definitive conclusion can be drawn but it is relevant to observe that NNDMA is an exceptionally good solvent and may well contribute to the low heterogeneity of these two materials. Comfilcon A and balafilcon A exhibit appreciably greater heterogeneity than their two counterparts and their respective macromer structures (Figure 1, structures 4a and 4b) appear to offer greater potential for hydrophobic clustering. Comfilcon A is characterized using both N-methyl-N-vinyl acetamide and NNDMA which contrasts with balafilcon A which relies almost completely on the solvent power of N-vinyl pyrrolidone. These factors may well contribute to the difference in morphology—which is striking. The various process-related factors that govern cure

rates and kinetics of polymerization will also influence network formation and morphology but the nature and extent of these effects is not in the public domain. It is clear that differences in chemistry and morphology of these materials are interlinked and that further systematic studies will be necessary to resolve the detailed effects of structure on self-assembly.

The use of a series of techniques that probe different aspects of morphology and heterogeneity demonstrates that heterogeneity can lead to higher levels of ion permeability than are achieved with homogeneous hydrogels. This is a consequence of the way in which the aqueous domains are organized. It is through this investigation and understanding of the length scale of morphological self-assembly that we have been able to explain why the bulk picture of water content and water structure, which predicts ion and oxygen permeability in homogeneous hydrogels does not apply to the SiHys exemplified here. Our results suggest that "morphological heterogeneity" of the polymer phase explains what cannot be determined directly—the "morphological organization" of the aqueous phase.

5 | CONCLUSIONS

Figure 9 summarizes the investigative approach undertaken in this study. It illustrates the various structural length scales of the contact lenses, starting with the molecular composition of the polymer chains up to the bulk contact lens itself. This study reported the use of SAXS and ESEM to probe, respectively, nanoscale and mesoscale morphologies which are inevitably a function of the chemistry, composition and process characteristics leading to self-assembly in these macromolecular materials. These approaches, taken together, have indicated why a group of SiHys with so many apparent similarities have such different electrolyte permeability characteristics. Just as oxygen permeability has been established as a primary requirement for corneal health, circumstantial evidence is growing that links ocular electrolyte composition to corneal homeostasis. This in turn indicates the potential importance of ion permeability of the contact lens in overcoming the occurrence of corneal adverse events.

This work was designed to probe and explain the characteristics of a set of commercial SiHys. Because of the lack of information specifically linking commercial products to information in the relevant patents, it is difficult to directly correlate the observed behavior with each specific individual component. It is clear from the way that new products have been developed, and islands of intellectual property defined and defended, that a huge amount of knowledge and understanding exists within commercial companies.[19] The limited amount of public domain information underlines the fact that the relationships between structure and performance that exist between the varied and versatile structural components that characterize this group of biomaterials are currently unexplored and unexploited for other applications. However, that fact provides a logical impetus to study structure–property relationships of purpose-synthesized silicone-based copolymers. The ability to manipulate and predict the structure and physical properties of a polymer network by changing specific variables (i.e., polymer molecular weight and concentration, chemical groups, initiator, cross-linker and polymerization method) is fundamental to the successful development of any process.

ORCID
Aisling Mann https://orcid.org/0000-0002-4075-8831
Paul D. Topham https://orcid.org/0000-0003-4152-6976

REFERENCES
1. Richdale K, Sinnott LT, Skadahl E, Nichols JJ. Frequency of and factors associated with contact lens dissatisfaction and discontinuation. *Cornea*. 2007;*26*:168-174.
2. Young G, Veys J, Coleman S. A multicentre study of lapsed contact lens wearers. *Optom Physiol Opt*. 2002;*22*:516-527.
3. Nichols JJ, Willcox MD, Bron AJ, et al. The TFOS international workshop on contact lens discomfort: executive summary. *Invest Ophthalmol Vis Sci*. 2013;*54*:TFOS7-TFOS13.
4. Domschke A, Lohmann D, Winterton L. On-eye mobility of croft oxygen permeable contact lenses. Paper presented at: Proceedings of ACS Spring National Meeting, PMSE, San Francisco, CA; 1987.
5. Tighe BJ, Mann AM. Contact lens materials. In: Phillips AJ, Speedwell L, eds. *Contact Lenses*. 6th ed. Amsterdam, the Netherlands: Elsevier Health Sciences; 2019:18-32.
6. Papas EB. The significance of oxygen during contact lens wear. *Cont Lens Ant Eye*. 2014;*37*:394-404.
7. Golebiowski B, Papas EB, Stapleton F. Corneal and conjunctival sensory function: the impact on ocular surface sensitivity of change from low to high oxygen transmissibility contact lenses. *Invest Ophthalmol Vis Sci*. 2012;*53*:1177-1181.
8. Tighe BJ. Silicone hydrogels: structure, properties and behaviour. Sweeney DF, editor. *Silicone Hydrogels: Continuous Wear Contact Lenses*. Edinburgh, UK: Butterworth-Heinemann; 2004:1–27.
9. Thaysen JH, Thorn NA. Excretion of urea, sodium, potassium and chloride in human tears. *Am J Physiol*. 1954;*178*:160-164.
10. Polse KA. Tear flow under hydrogel contact lenses. *Invest Ophthalmol Vis Sci*. 1979;*18*:409-413.
11. Mahomed A, Tighe BJ. 2015 corneal health and contact lens wear: ion chromatography as an electrolyte probe. *Cont Lens Ant Eye*. 2015;*38*:e20.
12. Mann AM, Tighe BJ. Contact lens interactions with the tear film. *Exp Eye Res*. 2013;*117*:88-98.
13. Mann AM, Sáez-Martinez V, Lydon F, Tighe BJ. Investigating the permeation properties of contact lenses and its influence on tear electrolyte composition. *J Biomed Mater Res B Appl Biomater*. 2019;*107*: 1997-2005.
14. McNamara NA, Polse KA, Brand RJ, Graham AD, Chan JS, McKenney CD. Tear mixing under a soft contact lens: effects of lens diameter. *Am J Ophthalmol*. 1999;*127*:659-665.
15. Nichols JJ, Mitchell GL, King-Smith PE. Thinning rate of the precorneal and prelens tear films. *Invest Ophthalmol Vis Sci*. 2005;*46*: 2353-2361.

16. Muntz A, Subbaraman LN, Sorbara L, Jones L. Tear exchange and contact lenses: a review. *J Optom*. 2015;8:2-11.

17. Szczotka-Flynn L, Diaz M. Risk of corneal inflammatory events with silicone hydrogel and low Dk hydrogel extended contact lens wear: a meta-analysis. *Optom Vis Sci*. 2007;84:247-256.

18. Guan L, Gonzalez Jimenez ME, Walowski C, Boushehri A, Prausnitz JM, Radke CJ. Permeability and partition coefficient of aqueous sodium chloride in soft contact lenses. *J Appl Polym Sci*. 2011;122:1457-1471.

19. Nicolson PC, Vogt J. Soft contact lens polymers: an evolution. *Biomaterials*. 2001;22:3273-3283.

20. Hamley IW. *The Physics of Block Copolymers*, Oxford, UK: . Oxford University Press; 1998.

21. Adams DJ, Topham PD. In: Steed JW, Gale PA, eds. *Assembly of Block Copolymers in Supramolecular Chemistry: From Molecules to Nanomaterials*. Chichester, UK: John Wiley & Sons Ltd; 2012:3235-3254.

22. Lee KM, Kim KH, Yoon H, Kim H. Chemical design of functional polymer structures for biosensors: from nanoscale to macroscale. *Polymers*. 2018;10:551.

23. Arkles BC, Larson GL. *Silicon Compounds: Silanes and Silicones: A Survey of Properties and Chemistry*. Morrisville, PA: Gelest, Inc; 2008.

24. Nicolson P, Baron R, Charbrereck P, et al. Extended wear ophthalmic lens. 1999;US5965631.

25. Almond SL, Browning J. Conditions and methods for producing silicone hydrogel contact lenses. 2005;EP1752796B1.

26. Zanini D, Altheim K. Process for forming clear, wettable silicone hydrogel articles. 2006;US8507577B2

27. Bambury RE, Seelye DE. Novel vinyl carbonate and vinyl carbamate contact lens material monomers. 1989;US5070215.

28. Preziosi V, Perazzo A, Tomaiuolo G, Guido S. Flow-switchable morphology of concentrated emulsions. *Chem Eng Process*. 2018;125:275-279.

29. https://imagej.nih.gov/ij/download.html.

30. Fan L, Degen M, Bendle S, Grupido N, Ilavsky J. The absolute calibration of a small-angle scattering instrument with a laboratory x-ray source. *J Phys Conf Ser*. 2010;247(012005):1-10.

31. Murphy SM, Hamilton CJ, Tighe BJ. Synthetic hydrogels: 5. Transport processes in 2-hydroxyethyl methacrylate copolymers. *Polymer*. 1988;29:1887-1893.

32. Castellino V, Edgar Acosta E, Cheng Y-L. Interpenetrating polymer networks templated on bicontinuous microemulsions containing silicone oil, methacrylic acid, and hydroxyethyl methacrylate. *Colloid Poly Sci*. 2013;291:527-539.

33. Zhao Z, Xie H, An S, Jiang Y. The relationship between oxygen permeability and phase separation morphology of the multicomponent silicone hydrogels. *J Phys Chem B*. 2014;118(50):14640-14647.

34. Mansur HS, Sadahira CM, Souza AN, Mansur AAP. FTIR spectroscopy characterization of poly (vinyl alcohol) hydrogel with different hydrolysis degree and chemically crosslinked with glutaraldehyde. *Mat Sci Eng C*. 2008;28:539-548.

35. Topham PD, Howse JR, Crook CJ, et al. Autonomous volume transitions of a polybase triblock copolymer gel in a chemically driven pH-oscillator. *Macromol Symp*. 2007;256:95-104.

36. Blanazs A, Verber R, Mykhaylyk O, et al. Sterilizable gels from thermoresponsive block copolymer worms. *J Am Chem Soc*. 2012;134:9741-9748.

37. Seitz ME, Wiseman ME, Hilker I, et al. Influence of silicone distribution and mobility on the oxygen permeability of model silicone hydrogels. *Polymer*. 2017;118:150-162.

38. Nightingale ER. Phenomenological theory of ion solvation, effective radii of hydrated ions. *J Phys Chem*. 1959;63:1381-1387.

39. Weast RC, Astle MJ, Beyer WH. *CRC Handbook of Chemistry and Physics*. 66th ed. Boca Raton, FL: CRC Press; 1986.

40. Rieger PH. *Electrochemistry*. New York, NY: Springer International Publishing; 1994.

41. Mason PE, Brady JW. "Tetrahedrality" and the relationship between collective structure and radial distribution functions in liquid water. *J Phys Chem B*. 2007;111:5669-5679.

42. Franks F. *Water, a Matrix of Life*. 2nd ed. Gateshead, UK: Athenaeum Press Ltd; 2000.

43. Gido S. Morphological characterization of silicone hydrogels. Paper presented at: APS March Meeting (Vol 52, no. 1), BAPS 2007;MAR. L24.2.

44. Mamodia M, Panday A, Gido SP, Lesser AJ. Effect of microdomain structure and process conditions on the mechanical behavior of cylindrical block copolymer systems. *Macromolecules*. 2007;40:7320-7328.

45. Embleton JK, Tighe BJ. Polymers for biodegradable medical devices. X. Microencapsulation studies: control of poly-hydroxybutyrate-hydroxyvalerate microcapsules porosity via polycaprolactone blending. *J Microencapsul*. 1993;10:341-352.

46. Oxley HR, Corkhill PH, Fitton JH, Tighe BJ. Macroporous hydrogels for biomedical applications: methodology and morphology. *Biomaterials*. 1993;14:1064-1072.